Plasma Wave Source Location Using CLUSTER as a Spherical Wave Telescope

O.D. Constantinescu[1,2], K.-H. Glassmeier[1], U. Motschmann[3], R. A. Treumann[4], and M. Fränz[5]

[1]Institut für Geophysik und extraterrestrische Physik, Braunschweig
[2]Institute for Space Sciences, Bucharest
[3]Institute of Theoretical Physics, Braunschweig
[4]Max-Planck-Institut für extraterrestrische Physik, Garching
[5]Max-Planck-Institut für Sonnensystemforschung, Lindau

July 4, 2006

Abstract

The use of sensor arrays in space opens up the possibility to investigate the source location of plasma waves. In order to do so we generalize the wave telescope technique to use spherical waves instead of plane waves. The new tool determines the center of the wave fronts locally measured by the sensor array. This virtual source can be related with the position of the real source generating the detected waves provided the wave propagation mode and medium properties are known. Moreover, the motion of the source region can be derived, as well as its basic geometrical characteristics. In this work we give the theoretical background for the new tool and examples of location analysis based on synthetic data. An example based on CLUSTER magnetic field data in the day side magnetosheath reveals a virtual source region elongated in the magnetic field direction, moving with the plasma flow in the vicinity of the spacecraft configuration.

1 Introduction

To fully exploit the observations gained by extended ground based magnetometer arrays (e.g. Küppers et al., 1979) or multi-point measurements in space such as measurements provided by the CLUSTER spacecraft fleet (Escoubet et al., 1997) regular data mining techniques such as Fourier spectral analysis or wavelet analysis are often not sufficient. More powerful tools (e.g. Glassmeier, 1980; Glangeaud and Latombe, 1983; Samson, 1983; Balikhin et al., 2003) are required and have been applied successfully. For analysis of CLUSTER observations Pinçon and Lefeuvre (1991); Lefeuvre and Pinçon (1992); Motschmann et al. (1995); Glassmeier et al. (2001); Sahraoui et al. (2003) have developed and applied the so-called k-filtering or wave telescope technique. This method uses plane waves representation to analyze the measured wave field and derive

important properties like propagation direction, wave length and dispersion relation (e.g. Narita et al., 2003; Schäfer et al., 2005). Recently, Tjulin et al. (2005) used for the first time the combined electric and magnetic field measured by CLUSTER for the first application to real data of the k-filtering technique as described by Pinçon and Lefeuvre (1991).

While the plane waves representation has multiple advantages, it also limits the applicability of the wave telescope to the far field case. As a result, this method cannot directly answer fundamental questions related to the sources of the measured field. Examples are finding the positions of the wave sources, their motion or their geometrical characteristics. If these questions are to be answered, we have to give up the plane waves representation in favor of a representation which takes into account the distance to the wave source, such as the spherical waves representation.

In what follows we show how a generalization of the wave telescope technique to spherical waves representation appears naturally. First, we establish the theoretical framework and we analyze different scenarios like geometrically extended sources and source motion relative to the sensor array or to the plasma background. Next we use synthetic data to illustrate these situations. Finally we show an example where the spherical wave representation is used to locate a wave source in the magnetosheath and to draw conclusions about its motion and shape.

Before we start to discuss in more detail the new proposed data representation method some more general comments are suitable. What we are proposing here is a representation technique of a given wave field as seen by e.g. the CLUSTER spacecraft. This representation is a local one. No information about the global system the wave has been generated and has propagated through is immediately available and used. This involves, of course, limitations. For instance, we do not take into account any consideration on the anisotropy characteristics of waves propagating in magnetized plasma. Also, we do not take into account complexity as introduced by the background medium being inhomogeneous. Furthermore, we disregard for the time being any information about wave polarization properties. The aim of our presented approach is to provide an extension of the already in-use techniques to analyze CLUSTER data such as the k-filtering technique (Lefeuvre and Pinçon, 1992), the wave telescope (Motschmann et al., 1995) or the phase differencing method (Balikhin et al., 2003). Compared to the existing tools, the new tool provides information about the local curvature of the wave fronts. This can be used to determine the local curvature center hereafter called "virtual source". The exact relation between the virtual source and the real wave source is determined by the factors enumerated above. Apart for simple cases, inferring the real source position from the virtual one is far from trivial and is beyond the purpose of this paper.

Relaxing on the condition of using a plane wave representation already increases the complexity of the tool and of the interpretation of its results very much. Thus we omitted any inclusion of medium and wave mode related considerations. This will and must be the next step to be done. A more detailed discussion on effects related to wave polarization, but using single spacecraft observations can be found in e.g. Storey and Lefeuvre (1979) where the concept of a wave distribution function is introduced. However, the use of this method requires to decompose the detected wave field into known plasma wave modes. A recent application has been presented by Santolík and Gurnett (2002). A

generalization of these concepts to multi-point measurements has not yet been presented.

2 Theoretical Framework

Assume that the measured field $X(\boldsymbol{r},t)$ is a superposition of elementary waves $w(\boldsymbol{q},\boldsymbol{r},t)$ where $\boldsymbol{q}=(q_1,\ldots,q_M)^T$ are the parameters of the elementary wave. The boldface characters represent column vectors and the superscript ^{T} indicates the transposition. A sensor positioned at $\boldsymbol{r}_{\text{sensor}}$ in a wave field generated by N elementary waves with parameters $\boldsymbol{q}_1 \ldots \boldsymbol{q}_N$ will measure the field

$$X(\boldsymbol{r}_{\text{sensor}},t) = \sum_{\substack{n=1 \\ \text{sources}}}^{N} c_n w(\boldsymbol{q}_n,\boldsymbol{r}_{\text{sensor}},t) \tag{1}$$

We define the array output for the set of parameters $\boldsymbol{q}$ as the projection of the measured field on the elementary wave corresponding to the set of parameters $\boldsymbol{q}$:

$$X_A(\boldsymbol{q}) = \langle w(\boldsymbol{q},\boldsymbol{r}_{\text{sensor}},t)|X(\boldsymbol{r}_{\text{sensor}},t)\rangle_{\boldsymbol{r}_{\text{sensor}},t} \tag{2}$$

with the notation

$$\langle f(\alpha)|g(\alpha)\rangle_\alpha = \begin{cases} \int f^\star(\alpha)g(\alpha)d\alpha & \text{for continuous } \alpha \text{ values,} \\ \sum_j f^\star(\alpha_j)g(\alpha_j) & \text{for discrete } \alpha \text{ values.} \end{cases} \tag{3}$$

The * denotes complex conjugation.

If the system of elementary waves is normalized and chosen to be orthogonal, i.e.

$$\langle w(\boldsymbol{q},\boldsymbol{r},t)|w(\boldsymbol{q}',\boldsymbol{r},t)\rangle_{\boldsymbol{r},t} = \delta(\boldsymbol{q}-\boldsymbol{q}') \tag{4}$$

the array output becomes:

$$X_A(\boldsymbol{q}) = \sum_{\substack{n=1 \\ \text{sources}}}^{N} c_n \delta(\boldsymbol{q}-\boldsymbol{q}_n) \tag{5}$$

We define the array output power as the squared norm of the array output:

$$P(\boldsymbol{q}) = \|X_A(\boldsymbol{q})\|^2 \tag{6}$$

The above defined power differs from zero only when the set of parameters $\boldsymbol{q}$ coincides with the parameters of one of the elementary waves generating the wave field. Assuming that each elementary wave is associated with a source, the power corresponding to the source n, $P(\boldsymbol{q}_n)=|c_n|^2$, represents the contribution of that source to the wave field. In principle all we have to do in order to identify the sources is to scan the parameter space and search for power maxima. In practice the scanning procedure uses finite steps in parameter space. This corresponds to a reduction of the original set $\{w(\boldsymbol{q},\boldsymbol{r},t)\}$ which normally covers an infinite number of elementary waves to a finite set where only the scanned $\boldsymbol{q}$ values appear.

When the array consists of only one sensor and we choose the elementary waves to be plane waves

$$w(\omega, t) = \frac{1}{\sqrt{2\pi}} e^{-i\omega t} \tag{7}$$

our analysis is reduced to Fourier analysis. In this case the parameter space $\{\boldsymbol{q}\} = \{\omega\}$ is the one dimensional frequency space.

Let us assume in the general case that the temporal dependence of the elementary wave is of the form stated by equation (7) and can be separated:

$$w(\boldsymbol{q}, \omega, \boldsymbol{r}_{\text{sensor}}, t) \doteq w(\boldsymbol{q}, \boldsymbol{r}_{\text{sensor}}) w(\omega, t) \tag{8}$$

To simplify the notation, here and in the following $w(\dots)$ always denotes our elementary wave. When depending on different arguments, $w(\dots)$ represents different functions. For instance $w(\omega, t)$ is not the same function as $w(\boldsymbol{r}, k)$. Because the projection on the vector $|w(\omega, t)\rangle$ results in the Fourier transform

$$\langle w(\omega, t) | f(t) \rangle_t = \tilde{f}(\omega) \tag{9}$$

the array output becomes:

$$X_A(\boldsymbol{q}, \omega) = \left\langle w(\boldsymbol{q}, \boldsymbol{r}_{\text{sensor}}) | \tilde{X}(\boldsymbol{r}_{\text{sensor}}, \omega) \right\rangle_{\boldsymbol{r}_{\text{sensor}}} \tag{10}$$

which means that we can first Fourier analyze the measured data and then continue the analysis in the Fourier space. This is important in practice since it reduces the dimension of the space to be scanned.

2.1 Beamformer

The sensor positions $\{\boldsymbol{r}_{\text{sensor}}\}$ are discrete. This allows us to write equation (10) in a more familiar vector notation:

$$X_A(\boldsymbol{q}, \omega) = \sum_{\substack{s=1 \\ \text{sensors}}}^{S} w_s^\star(\boldsymbol{q}) \tilde{X}_s(\omega) = \boldsymbol{w}^\dagger(\boldsymbol{q}) \cdot \tilde{\boldsymbol{X}}(\omega) \tag{11}$$

where $\boldsymbol{x}^\dagger$ is the hermitian adjoint of $\boldsymbol{x}$.

If we choose plane waves as our set of elementary waves ($\boldsymbol{q} = \boldsymbol{k}$)

$$w_{\text{sensor}}(\boldsymbol{k}) = \frac{1}{\sqrt{S}} e^{i\boldsymbol{k}\cdot\boldsymbol{r}_{\text{sensor}}} \tag{12}$$

then equations (11) and (6) constitute nothing more then the beamformer technique (Pillai, 1989). If enough sensors are available, using the beamformer technique we can decompose the measured signal into plane waves with known wave vectors and frequencies.

We have to be aware that because we have discretised the position space (which we have to, since we do not have sensors at each point in space) our set of elementary waves is no longer a complete system. As a consequence, the δ function in equation (5) becomes just a function with local maxima for $(\omega, \boldsymbol{k})$ close to the sets $(\omega_n, \boldsymbol{k}_n)$ of sources generating the measured wave field. The less sensors we have, the more important this effect becomes. Moreover, side lobes begin to appear. For the particular case of the CLUSTER spacecraft, with only four sensors, the beamformer method as described above becomes useless. However, there are possibilities to reduce these effects which will be discussed in the following sections.

2.2 Wave Telescope

The weak point of the beamformer technique results from artificial contributions to the power at points in the parameter space which do not correspond to any real wave source. A remedy is to minimize these contributions while keeping the power corresponding to the real wave sources unmodified. This is accomplished by Capon's minimum variance estimator (Capon et al., 1967)

We have to find a new set of elementary waves $\{h(\boldsymbol{q})\}$ which satisfy the problem:

$$\min\|X_A\|^2 = \min_{|h\rangle} \langle h|X\rangle\langle X|h\rangle \quad \text{subject to} \quad \langle h|w\rangle = 1 \tag{13}$$

The new weights are found as

$$|h\rangle = \frac{(|X\rangle\langle X|)^{-1}}{\langle w|\,(|X\rangle\langle X|)^{-1}\,|w\rangle}\,|w\rangle \tag{14}$$

which gives the new expression for the power:

$$P = \Big[\langle w|\,(|X\rangle\langle X|)^{-1}\,|w\rangle\Big]^{-1} \tag{15}$$

For the plane waves representation (equation 12) and discrete position space the power becomes:

$$P(\omega,\boldsymbol{k}) = \big[\boldsymbol{w}^{\dagger}(\boldsymbol{k})\mathcal{M}^{-1}(\omega)\boldsymbol{w}(\boldsymbol{k})\big]^{-1} \tag{16}$$

The matrix elements $[\mathcal{M}(\omega)]_{ij}$ are obtained by averaging the quantities $\tilde{X}_i^{\star}(\omega)\tilde{X}_j(\omega)$ over a frequency band centered on ω. This mixing of frequencies normalizes the matrix $\mathcal{M}$ which would otherwise be singular. It also helps the analysis of sources emitting in a broad frequency range. However, this implies the assumption that the detected field is stationary in time and homogeneous in space.

The wave energy density in the wave vector space equivalent with equation (16) for an electromagnetic field can be also estimated from single point measurements of the electric and magnetic field using the wave distribution function method. Similarly with the kinetic theory of gases Storey and Lefeuvre (1979, 1980) describe the wave field as an ensemble of elementary plane waves characterized by a distribution function representing the average wave energy in the volume $\mathrm{d}\mathbf{r}\mathrm{d}\mathbf{k}$ at the point $(\mathbf{r},\mathbf{k})$. To compensate the lack of multiple instantaneous measurements in space this method assumes a priori knowledge of the dispersion relation.

For the sake of simplicity we have limited ourselves to scalar fields. Nevertheless, these considerations are easily extended to vector fields as well. For a vector field with an arbitrary dimension L we construct the $LS \times L$ elementary wave matrix $\mathcal{W}$ as

$$\mathcal{W}(\boldsymbol{k}) = \big(\mathcal{I}w_1(\boldsymbol{k}),\ldots,\mathcal{I}w_S(\boldsymbol{k})\big)^T \tag{17}$$

where $\mathcal{I}$ is the L dimensional unity matrix. We group the measurements into the LS dimension vector $\mathbf{X}(\boldsymbol{r},t)$ with the corresponding Fourier transform

$$\tilde{\mathbf{X}}(\omega) = \big(\tilde{\mathbf{X}}_1^T(\omega),\ldots,\tilde{\mathbf{X}}_S^T(\omega)\big)^T \tag{18}$$

The individual sensor measurements $\mathbf{X}_s$ consist of either one vector quantity such as the magnetic field in which case $L = 3$ or of a combination of quantities which oscillate coherently. As for an example we can combine the electric and the magnetic field in the six dimensional vector $\mathbf{X}_s = (\mathbf{B}_s^T, \mathbf{E}_s^T)^T$ (Pinçon and Lefeuvre, 1991; Tjulin et al., 2005). The power corresponding to the vector field is:

$$P(\omega, \boldsymbol{k}) = \text{trace}\left(\left[\mathcal{W}^\dagger(\boldsymbol{k})\mathcal{M}^{-1}(\omega)\mathcal{W}(\boldsymbol{k})\right]^{-1}\right) \tag{19}$$

When applied to a magnetic field measured in space this method is known as the wave telescope or k-filtering (e.g. Pinçon and Lefeuvre, 1991; Motschmann et al., 1995; Pinçon and Motschmann, 1998; Glassmeier et al., 2001). It has been proved to be a robust method to determine the $\boldsymbol{k}$ vector from magnetic field measurements. Nevertheless, while it gives us the propagation direction, it provides no information about the distance to the source generating the wave. This is inherent to the plane waves representation.

2.3 Source Locator

In order to determine the sources locations we have to choose a system of elementary waves which contains information about the distance to the source. The most natural (and simple) choice is the spherical waves representation where the elementary waves are characterized by $\boldsymbol{q} = (\boldsymbol{r}_{\text{source}}, k, \omega) = (\boldsymbol{r}, k, \omega)$ representing the position, wave number, and frequency of the source. Thus for the sensor s at the position $\boldsymbol{r}_s$ one gets

$$w(\boldsymbol{r}, k, \omega, \boldsymbol{r}_s, t) = C\frac{1}{\rho_s}e^{i(k\rho_s - \omega t)} \tag{20}$$

where $\rho_s = \rho(\boldsymbol{r}_s, \boldsymbol{r}) = |\boldsymbol{r}_s - \boldsymbol{r}|$ is the distance between the source and the sensor s. The elementary wave associated to the sensor s becomes after separation of the time dependent part

$$w_s(\boldsymbol{r}, k) = C\frac{1}{\rho_s}e^{ik\rho_s} \tag{21}$$

The normalization coefficient is:

$$C = \left(\sum_{\substack{s=1 \\ \text{sensors}}}^{S} \frac{1}{\rho_s^2}\right)^{-1/2} \tag{22}$$

Even if the single-sensor elementary wave w_s depends only on the distance ρ_s between source and sensor, the vector $\boldsymbol{w} = (w_1, \ldots, w_S)^T$ depends on $\boldsymbol{R} = (\rho_1, \ldots, \rho_S)^T$ which is a function of the source position. As a consequence, the array power, which has the same formal expression as for the wave telescope (equation 16), will also depend on the source position.

$$P(\omega, \boldsymbol{r}, k) = \left[\boldsymbol{w}^\dagger(\boldsymbol{r}, k)\mathcal{M}^{-1}(\omega)\boldsymbol{w}(\boldsymbol{r}, k)\right]^{-1} \tag{23}$$

In contrast to the three dimensional parameter space of the wave telescope $\{\boldsymbol{q}\} = \{\boldsymbol{k}\}$, the parameter space of the source locator $\{\boldsymbol{q}\} = \{\boldsymbol{r}_{\text{source}}, k\}$ is four dimensional. As for the wave telescope, in order to find the source parameters

we have to scan the parameter space in order to determine the array power at each point of a grid and identify the power maxima.

The scan domain in the position space can formally be extended to $0 < \rho < \infty$ but the more distant the source is, the more the observed wave will approach a plane wave and the uncertainty in determining the distance will increase. For the wavelength (k-number) space we shall take into consideration the Nyquist theorem otherwise aliasing occurs. It is possible to define the maximum wave number as a function of propagation direction (e.g. Neubauer and Glassmeier, 1990; Pinçon and Motschmann, 1998; Glassmeier et al., 2001) but we chose the simple approach $k \leq k_{\mathrm{Nyquist}} = \pi/d_{\mathrm{max}}$, d_{max} being the maximum spacecraft separation.

The resulting array power is a local representation of the wave field. The position $\boldsymbol{r}$ derived from the array power maximum represents the center of spherical shells determined by the source locator by analyzing the local curvature of the wave fronts and the spatial decay of the field. This position is associated with a virtual source which generally differs from the real source. The two coincide only when the wave isotropically propagates in an homogeneous medium. In order to relate the position of the virtual source to the position of the real source we have to extrapolate our local knowledge of the propagation medium and to take into account the mode in which the waves propagate. This differs from case to case and no general recipe can be given. As for an example for fast magnetosonic waves the position of the virtual source is a good approximation of the position of the real source but this is not true for an Alfvén wave. An example on how the real source position can be determined from the virtual source position when the wave propagates anisotropically is given in section (3.3). It follows that a complete source location analysis would consist of two steps. First, determine the virtual source position using a general procedure, second, link this position to the real wave source using wave mode analysis and medium related considerations. Since it is already far from trivial, we only cover the first step in this work. However, even without any knowledge about the propagation mode of the detected waves the tool is still able to distinguish between close and remote sources, the later being associated with plane waves.

3 Application to synthetic data

To test our new method we generate synthetic data to represent waves propagating into an homogeneous isotropic medium. In this case the virtual source determined by the source locator coincides with the real wave source. The data incorporates random noise with a maximum deviation of 10% of the signal amplitude. Also errors in the sensors positions up to 10% of their average separation are included in the data to be analyzed. The sampling frequency is 1 s and the interval length is 512 s.

For simplicity we will consider only one source generating the wave field. Multiple sources with different frequencies which can be separated by frequency filtering can easily be identified and their contribution to the total wave field can be estimated. If the frequencies cannot be resolved by Fourier analysis but they are still not identical then each source will be identified by its own peak in the array power. We are able to separate up to three different sources in this case. However, if two sources have identical frequencies, because of the interference

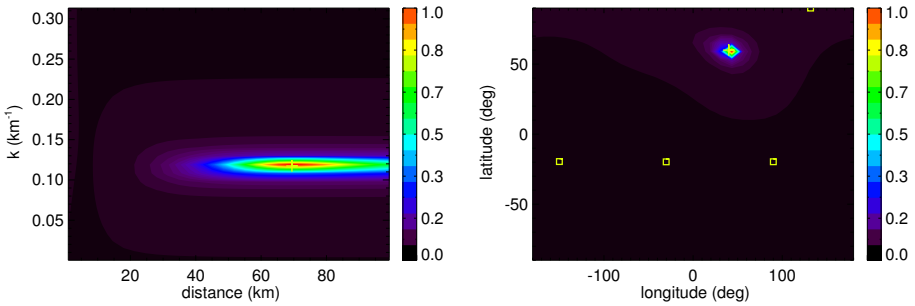

Figure 1: Normalized array power for the static case. The real location of the source is represented by the plus sign. In the longitude-latitude plot the spacecraft locations are represented by squares.

pattern which occurs the method cannot be applied anymore. This is also true for the wave telescope and related techniques. It is highly improbable to have separate sources which would be phase coherent. However, one could imagine scenarios having the same effect. For instance, detecting both the direct and the reflected wave originating from the same source is equivalent with detecting two phase coherent sources. A similar situation is encountered when the propagation medium is supersonically streaming as it will be shown in section (3.3).

The reference system we use is the array reference system which has its origin in the center of mass of the sensor array. The z axis goes through the most distant sensor and the next distant sensor belongs to the (x, z)-plane, $y \geq 0$. The x axis completes the system.

We compute the array power on a grid of dimensions $30 \times 30 \times 30 \times 30$. The first dimension is for the longitude of the source, ranging from $-180°$ to $180°$, the second dimension is for the latitude, from $-90°$ to $90°$, the third dimension is the distance from 0 to 10 spacecraft average separation distances and the fourth the wave number from 0 to k_{Nyquist}. For computing the $\mathcal{M}$ matrix we apply the fast Fourier transform to the data and average over five frequencies centered on the interest frequency, i.e. over $[\omega - 2\Delta\omega, \omega - \Delta\omega, \omega, \omega + \Delta\omega, \omega + 2\Delta\omega,]$ where $\Delta\omega = 2\pi$ rad/s

3.1 Static source

The synthetic data to be analyzed represents one source with a frequency of 100 rad/s positioned at a distance of 70 km from the spacecraft configuration center, a latitude of 60° and a longitude of 40°, measured by four sensors arranged in a near regular tetrahedron formation with a separation of about 10 km. The k-number of the synthetic wave is 0.11 km^{-1}. Both the source and the sensor array are at rest with respect to the propagation medium.

In Figure (1) we show location analysis results as two dimensional slices through the computed power. The plus sign represents the given location of the source and the squares in the longitude-latitude plot represent the sensors positions. The results are summarized in Table (1).

Looking at the distance-k plot we note that, even if the maximum power lies at the right position, it has an elongated shape in the distance dimension

	given	found
distance	70 km	69 km
longitude	40°	43°
latitude	60°	59°
k	0.11 km^{-1}	0.10 km^{-1}

Table 1: Results of source location analysis for the static case

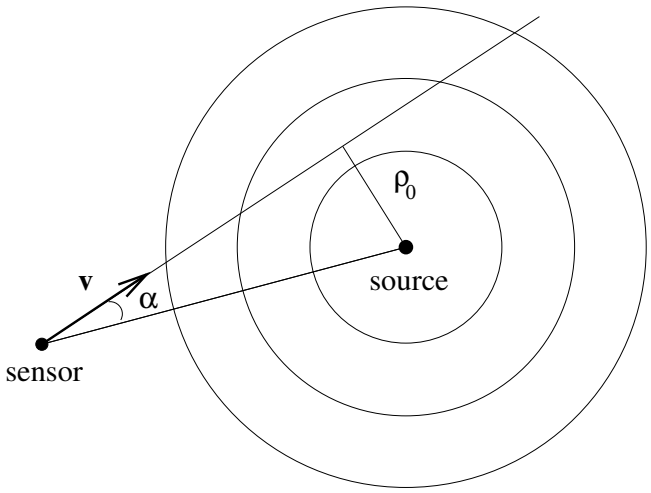

Figure 2: The sensor is moving with the velocity $\boldsymbol{v}$. The measured frequency depends on the angle α between the velocity and the direction to the source.

direction. This is due to the limited extent of the sensor array in the position space compared to the distance to the source. The closer the source is, the less elongated the peak is. From our experience, with a regular tetrahedron configuration we can distinguish between a spherical and a plane wave up to a distance of about 20 spacecraft separation distances.

We have shown that we can recover the location and the wave length of a given source using a CLUSTER type array of sensors when the source and the sensors are not moving with respect to the plasma frame. However, this is an idealized situation. The relative motion of the source with respect to the spacecraft formation and the plasma flow are creating distinct effects.

3.2 Sensor Motion

We now allow for relative motion between the sensor array and the wave source as in Figure (2) but not for motion of the source with respect to the plasma background. The measured magnetic field becomes

$$B = \frac{B_0}{\rho(t)} e^{i[k\rho(t) - \omega_0 t]}. \tag{24}$$

which leads to a time dependent Doppler shifted frequency given by

$$\omega(t) = \omega_0 \left[1 - \frac{v}{v_{\mathrm{ph}}} \cos\alpha(t) \right] \tag{25}$$

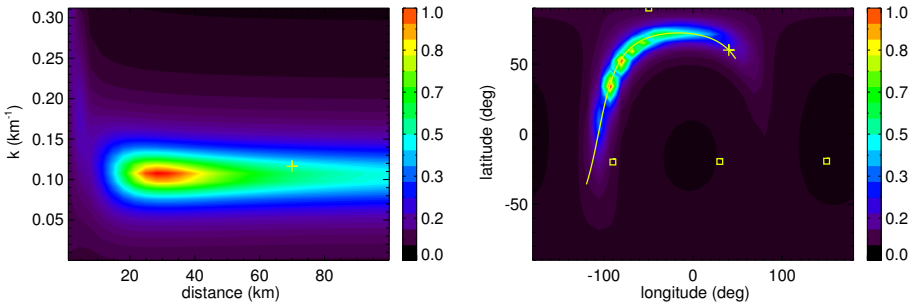

Figure 3: Array power when the sensors are moving with respect to the source. The array power maximizes in the vicinity of the closest approach rather than at the initial source location. The plus sign represents the initial source location and the squares represent the sensors locations. The line in the longitude-latitude plot represents the apparent source trajectory projection.

	initial location	found	closest approach
distance	70 km	28 km	21 km
longitude	40°	−93°	−91°
latitude	60°	34°	39°
k	0.11 km^{-1}	0.10 km^{-1}	0.11 km^{-1}

Table 2: Results of source location analysis when the sensors are moving with respect to the source.

In the above relations $\rho(t)$ is the distance between the sensor and the source, $\boldsymbol{v}$ is the sensor velocity, α is the angle between the velocity and the sensor−source direction and $v_{\text{ph}} = \omega_0/k$ is the wave phase velocity.

The sensor motion introduces differences compared to the static case. Not only the relative source position is changing over time but also the apparent frequency is now depending on time. Moreover, each sensor will measure slightly different frequencies. The sensors will record snapshots of the source position at the corresponding frequencies and the relative source motion will leave a trace in the array power.

As an example we apply location analysis to synthetic data representing a source having the same initial position and frequency as the one used for the static case (see Table 1) with the difference that this time the sensors are moving with a velocity of 171 km/s (roughly half of the wave phase velocity) in the direction (latitude = 55°, longitude = 44°). For this velocity the maximum Doppler shift is ±19% of the source frequency. Because of the Doppler effect, the Fourier power maximizes for a frequency of 110 rad/s which corresponds to an angle α of about 122° between the direction of motion of the source and the sensor to source direction. We use this frequency for our analysis. The closest approach is at a distance of 21 km at a longitude of −91° and a latitude of 39°. The distance-k and longitude-latitude cuts through the resulting array power are shown in Figure (3) and the results are summarized in Table (2).

The symbols in Figure (3) have the same meaning as the ones in Figure (1), in addition we have represented with a continuous line the projection of the

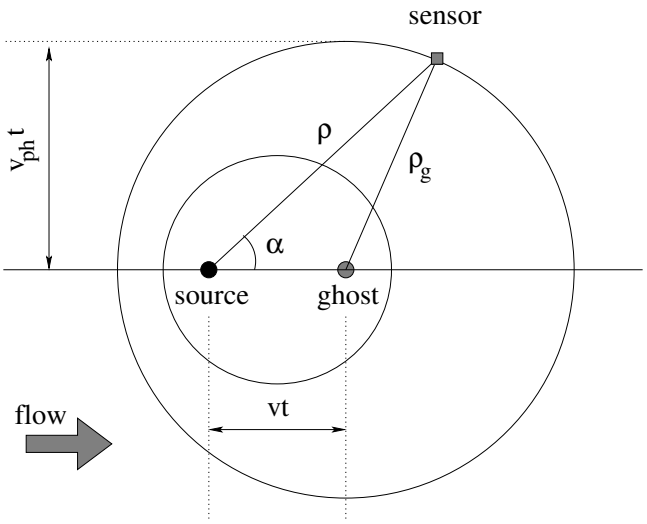

Figure 4: Subsonic plasma flow. The sensor is measuring a spherical wave apparently originating from the ghost source position. The measured frequency is the same as in the static case but the measured wave length depends on the angle α between the flow velocity and the source - sensor direction.

apparent motion of the source in the longitude-latitude plot. Unlike for the static case, the maximum array power is not localized but now stretched along the projection of the source trajectory. This is due to frequency mixing involved in computing the $\mathcal{M}$ matrix. Since a given frequency corresponds to a definite position of the source relative to the sensor, a range of frequencies is equivalent with a range of positions. In this case it corresponds to an angle between the direction of motion of the sensor and the relative direction to the source ranging from 48° to 132°. We also note that the array power reaches its maximum in the vicinity of the closest approach point and not near the initial position of the source (see Table 2). The characteristic signature of a moving source in the longitude-latitude plot can be identified in order to distinguish between static and moving sources. Together with equation (25) the source trace can in principle be used to determine the source velocity vector.

3.3 Plasma Flow

As we have seen in the previous section, when the sensor is moving with respect to the wave source, the measured frequency is no longer fixed but the measured wave length is the same as for the static situation. When plasma flow is present and the source does not move in the sensor reference frame, the opposite happens. The sensor will measure the same frequency as for the static case but the wave length is no longer fixed.

Figure (4) schematically represents the case for subsonic flow velocities. The wave front emitted at the moment $t = 0$ by the source is drifting with the plasma flow. By the time t when the wave front reaches the sensor it will be a sphere with a radius $v_{\rm ph}t$ and the center shifted at a distance vt from the source in the flow direction. With v we have denoted the plasma flow velocity and with

$v_{\text{ph}} = \omega/k_0$ the wave phase velocity in the absence of the flow. The presence of the flow introduces a preferred direction in the medium. The situation is equivalent with a change of the the wave phase velocity which now depends on the angle with the preferred direction, i.e. with anisotropic propagation through the medium.

We call the center of the wave front tangent to the sensor ghost source to differentiate it from a virtual source which has a shifted position from the real source due to "real" anisotropy of the medium. Apart from this the ghost source is the same as the virtual source defined in section (2.3).

The source locator will determine the ghost source position. From Figure (4) we have the following relation:

$$(v_{\text{ph}}t)^2 = \rho_{\text{g}}^2 = (vt)^2 + \rho^2 - 2vt\rho\cos\alpha \tag{26}$$

from which we can express the distance between the ghost source and the sensor

$$\rho_{\text{g}\pm}(\rho, \alpha, M) = \frac{\rho}{\xi_{\pm}(M, \alpha)} \tag{27}$$

with the notation

$$\xi_{\pm}(M, \alpha) = M\cos\alpha \pm \sqrt{1 - M^2\sin^2\alpha} \tag{28}$$

where $M = v/v_{\text{ph}}$ is the Mach number.

The magnetic field at the sensor position is

$$B(\rho, \alpha, M, t) = \frac{B_0}{\rho_{\text{g}}(\rho, \alpha, M)} e^{i[k_0\rho_{\text{g}}(\rho,\alpha,M) - \omega t]} \tag{29}$$

where k_0 is the wave number in the absence of the flow.

We can find the wave vector from the gradient of the magnetic field phase.

$$\boldsymbol{k}_{\pm}(M, \alpha) = \frac{k_0}{\xi_{\pm}} \left(\boldsymbol{e}_{\rho} \pm \frac{M\sin\alpha}{\sqrt{1 - M^2\sin^2\alpha}} \boldsymbol{e}_{\alpha} \right) \tag{30}$$

The corresponding wave number is

$$k_{\pm}(M, \alpha) = \frac{k_0}{\xi_{\pm}\sqrt{1 - M^2\sin^2\alpha}} \tag{31}$$

At a given sensor position, for subsonic flow only the '+' sign represents a physical solution and the field measured by the sensor is

$$B(\rho, \alpha, M, t) = \frac{B_0}{\rho_{\text{g}+}(\rho, \alpha, M)} e^{i[k_+\rho_{\text{g}+}(\rho,\alpha,M) - \omega t]} \tag{32}$$

However, when the flow reaches supersonic velocities, both solutions become valid inside the Mach cone. The '+' sign represents the advanced wave and the '$-$' sign the retarded wave.

As it can be seen in Figure (5), in the case of supersonic flow velocities, for each given source the sensor will measure waves apparently coming from two sources, the advanced and retarded ghosts:

$$B(\rho, \alpha, M, t) = \frac{B_0 e^{i[k_+\rho_{\text{g}+}(\rho,\alpha,M) - \omega t]}}{\rho_{\text{g}+}(\rho, \alpha, M)} + \frac{B_0 e^{i[k_-\rho_{\text{g}-}(\rho,\alpha,M) - \omega t]}}{\rho_{\text{g}-}(\rho, \alpha, M)} \tag{33}$$

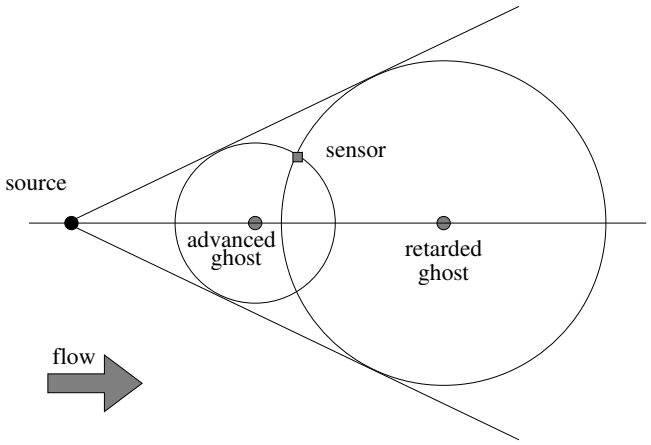

Figure 5: Supersonic flow. Both the advanced and retarded waves are measured by the sensor. The ghost sources locations depend on the Mach number and on the position of the sensor, therefore they are different from sensor to sensor.

This raises difficulties since the wave locator is unable to resolve coherent sources. However, as soon as the sensor begins to move with respect to the source it will measure different frequencies for the advanced and retarded ghosts and the problem disappears.

Solving equation (26) for t we find the arrival time (i.e. the time required for the wave to travel from the source to the sensor):

$$\tau_{\pm} = \frac{|\boldsymbol{r}_{\text{sensor}} - \boldsymbol{r}_{\text{source}}|}{v_{\text{ph}}\xi_{\pm}} \tag{34}$$

This allows us to write the ghost position vector:

$$\boldsymbol{r}_{\text{ghost}\pm} = \boldsymbol{r}_{\text{source}} + \boldsymbol{v}\tau_{\pm} \tag{35}$$

Again, whereas both solutions are valid inside the Mach cone for supersonic flows, for subsonic flows only the '+' solution is valid. Note that in contrast to the moving sensor case (section 3.3) the position of the ghost source is fixed with respect to the sensor but is different from sensor to sensor. This can have a negative impact on location analysis at high flow velocities if the source is very close to the sensor array.

We apply the location analysis to synthetic data representing a source with the same position and frequency as the static source in section (2.3), with the difference that the plasma is flowing with a velocity of 0.5 M with respect to both the source and the sensor array. The flow direction longitude is 175° and the latitude is −60°.

We show the array power in Figure (6) and the analysis results in Table (3). The dotted line in the longitude-latitude plot is representing the flow line going through the source and the diamonds are representing the ghost sources.

In the longitude - latitude plot the ghosts are grouped close to the flow line going through the real source and they are sliding away from it along the line as the flow velocity increases. If the flow velocity is known, equation (35) allows us to recover the direction to the real source.

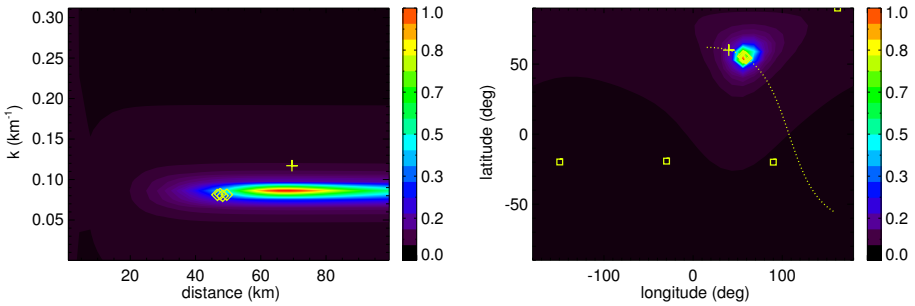

Figure 6: Array power when the plasma is flowing with 0.5 M with respect to the source. There is no relative motion between source and sensor array. The plus sign represents the source location, the diamonds the ghosts and the squares the sensors. The dotted line in the longitude-latitude plot represents the flow line through the source.

	real source	found	ghost
distance	70 km	68 km	48 km
longitude	40°	56°	58°
latitude	60°	53°	55°
k	0.11 km^{-1}	0.08 km^{-1}	0.08 km^{-1}

Table 3: Results of source location analysis for flowing plasma. The sensors are not moving. The ghost column shows averaged values over the sensors.

When the flow becomes supersonic, the retarded ghosts come into play making the analysis more difficult.

If in addition to the plasma flow we allow for the same sensor motion as in section (3.2), the ghosts will play the role of the real source and the power will maximize in the vicinity of the point of closest approach of the ghosts to the sensor array. The array power obtained in this case is shown in Figure (7) and we give the analysis results in Table (4).

3.4 Extended Source

Assume now the wave field is produced by a source having spatial extension and not being a point source. According to Huygens principle, the wave field produced by an extended source is the same as the wave field produced by a collection of point sources uniformly distributed over the space occupied by

	real source	found	closest ghost approach
distance	70 km	28 km	16 km
longitude	40°	−93°	−98°
latitude	60°	53°	43°
k	0.11 km^{-1}	0.07 km^{-1}	0.09 km^{-1}

Table 4: Results of source location analysis for flowing plasma and sensor motion. The ghost column shows averaged values over the sensors.

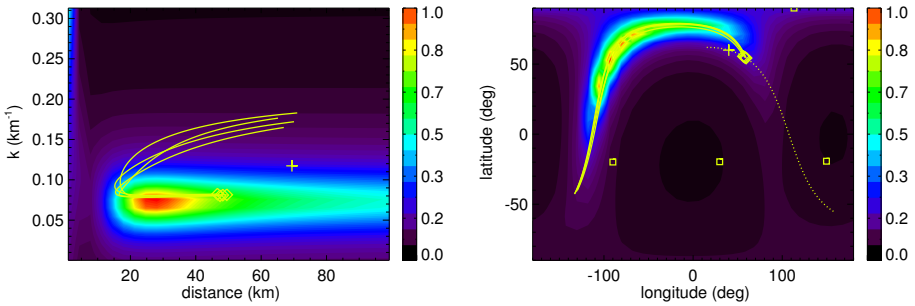

Figure 7: Array power in the presence of plasma flow when the sensor array is moving with respect to the source. The plus sign represents the source location, the diamonds the ghosts and the squares the sensors. The continuous lines represent the apparent motion of the ghosts and the dotted line in the longitude-latitude plot represents the flow line through the source.

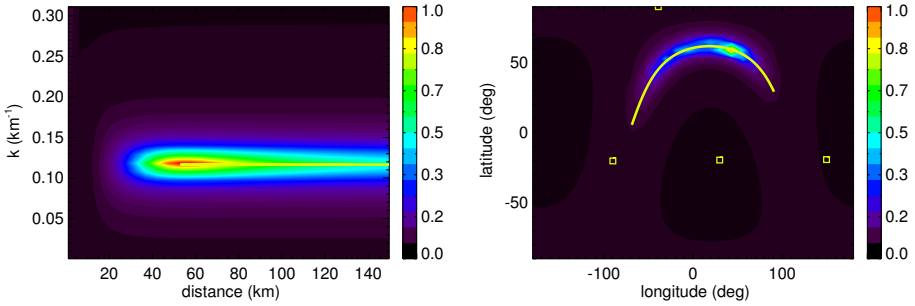

Figure 8: Array power for a static linear extended source. The source represented by the line in the longitude-latitude plot has a length of 30 km and is placed at 60 km away from the sensor array center.

the original source. This means that we should be able to identify an extended source and to gain information about its location and geometrical characteristics with the help of the source locator.

In order to check this hypothesis we apply location analysis to synthetic data representing a wave field generated by a standing linear source with a length of 30 average spacecraft separation distances, oriented along a longitude of 100° and a latitude of 15° and placed at a distance of 6 average spacecraft separation distances. The emitted power is uniformly distributed along the source.

As it can be seen in Figure (8) the source locator is indeed able to recover the original source. The position of the array power maximum as well as the position of the source center are given for comparison in Table (5).

When the sensor array is moving, the array output might not represent anymore the source geometry if the source is moving fast and close to the array. If we apply location analysis to the same extended source as in the previous example but with a non zero sensor velocity, instead of recovering the source geometry we get an array power maximum which is elongated in the direction

	source center	found
distance	60 km	57 km
longitude	40°	43°
latitude	60°	59°
k	0.11 km^{-1}	0.11 km^{-1}

Table 5: Results of source location analysis for a static linear extended source.

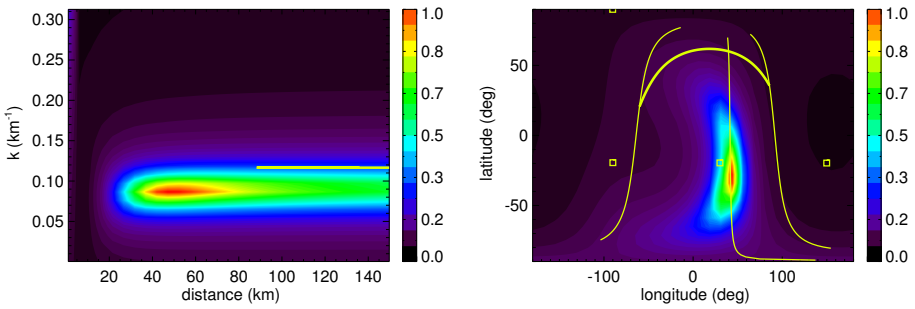

Figure 9: Array power for a linear extended source. The sensors are moving with a velocity of 171 km/s in the direction of 35° longitude and 79° latitude. The apparent motion of the middle and end points of the source are represented by the thin lines while the source itself is represented by the thick line in the longitude-latitude plot.

of motion. As a matter of fact, we see a trace of the source point closest to the sensor array. We show the corresponding array power in Figure (9). The thick line represents the source, the thin lines represent the motion of the middle and end points of the extended source.

If plasma flow is present the source locator will recover in a similar fashion the position of the ghost source but if the sensor array is also moving, the results cannot unambiguously be interpreted.

3.5 Remarks

We have seen that the source locator can give us information about the sources which are generating the measured wave field for various scenarios. However, when we have to analyze real data, the difficulty lies in differentiating between these situations.

Physical insight and a priori assumptions can be used to rule out some scenarios. As for an example, if we assume we are measuring a field produced by a magnetic structure frozen into the plasma we can rule out the scenario in section (3.3) describing the plasma flow in respect to the source.

On the other hand, the signatures of the array power in the section plots can give us a hint about which situation we are in. The shape of the power maximum in the k-angle plots is a measure of the dependence of the wave number on the direction. In other words, a symmetrical shape of the power maximum in the k-angle plots means that the wave isotropically propagates through the medium and it probably comes from a source at rest with respect to the plasma frame.

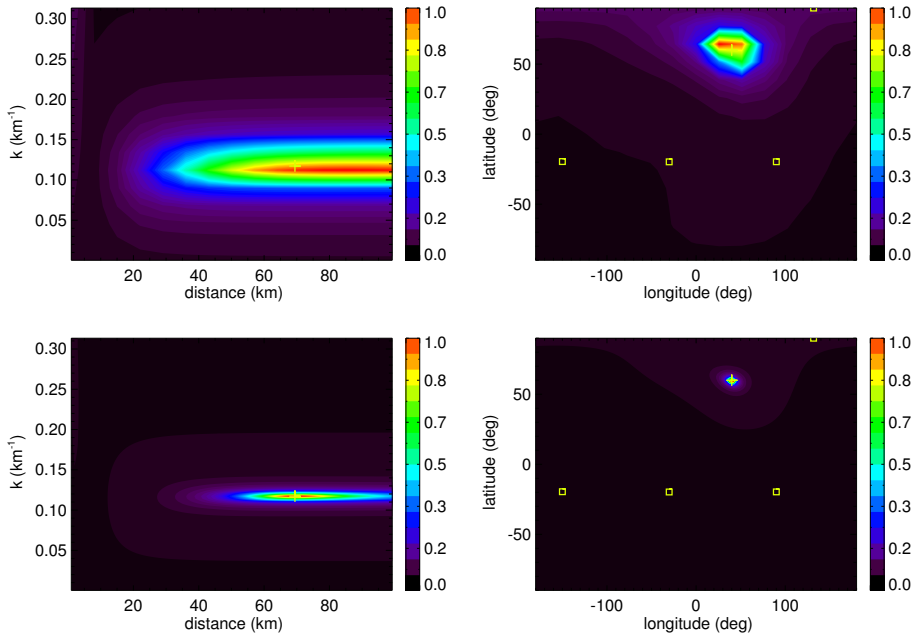

Figure 10: Source location results for the same data representing the static source in section 3.1 using different grid resolutions. The upper panels show the $15 \times 15 \times 15 \times 15$ and lower ones the $100 \times 100 \times 100 \times 100$ grid resolution results. The results in section 3.1 are obtained with a $30 \times 30 \times 30 \times 30$ grid resolution.

An asymmetrical shape in a k-angle plot tells us that either the propagation pattern of the wave is not isotropic, the source is moving with respect to plasma background, or we are dealing with an extended source.

The array power for moving sensors or for linear sources have very distinctive signatures in the latitude-longitude plots. These signatures resemble a sine-function and are the projection of a straight line on the longitude-latitude map. The ambiguity appears because we are dealing with an inverse problem, i.e. an unique set of measurements can correspond to several physical situations. For instance, the sine-function signature might also be produced by an homogeneous distribution of wave sources if the waves are only propagating orthogonal to a given direction. This is why the interpretation of the source locator results needs a careful analysis. To differentiate between a linear and a moving point source we can for example apply the source locator to the same data interval for different frequencies. If the field is produced by a moving source, because of the Doppler effect, different frequencies will represent the source on different positions on its trajectory. Also, comparing the orientation of the longitude-latitude trace with relevant directions like the local flow velocity or the background magnetic field direction can prove to be useful.

We should also keep in mind that the output of the source locator represents a virtual source, which still has to be related to the real source by analyzing the wave propagation mode.

The accuracy of the source locator is affected by the same factors affecting the accuracy of the wave telescope. One source of errors is the violation of the stationarity and homogeneity conditions. Statistical errors in the field measurements also affect the accuracy of the tool, leading to a decreased resolution but are not affecting the positions of the maxima. The scales to be investigated (wave lengths, source distance) have to be of the same order as the characteristic spacecraft separation. Otherwise spatial aliasing occurs for scales smaller than the configuration scale or the resolution decreases substantially for larger scales. One important factor is the array geometry. Large deviations from a three dimensional configuration – measured by the configuration quality index (Robert et al., 1998) – such as a very elongated or very flat array configurations affect the quality of the results. Pinçon and Lefeuvre (1992) discussed in detail the effects of the array geometry as well as of the errors in time synchronization and spacecraft position on the reliability of the wave telescope.

Of course, the resolution of the tool cannot be higher than the scanning grid resolution. If the grid is too loose and the source is very localized (i.e. the wave energy is concentrated in a very small domain in the $(k, \boldsymbol{r})$ space) the tool will not accurately locate the wave source. This is illustrated in Figure 10 where we show the results of a location analysis performed on the same data we used in section 3.1 for a stationary source with different grid resolutions.

The grid resolution $15 \times 15 \times 15 \times 15$ is too small and the error in locating the source is even larger than the grid resolution. However, the high resolution $100 \times 100 \times 100 \times 100$ gives basically the same results as the $30 \times 30 \times 30 \times 30$ used in section 3.1. Both the shape and location of the maximum are only minimally affected by increasing the grid resolution over $30 \times 30 \times 30 \times 30$ (see figure 1).

The grid resolution strongly affects the CPU time and computer memory needed for the analysis. These are proportional to the number of grid points used which have a power law dependence on the parameter space dimension (3 for the wave telescope, 4 for the source locator).

4 Application to CLUSTER data

To illustrate the potential of the source locator we analyze the magnetic field magnitude measured by the Fluxgate Magnetometer (FGM) instrument (Balogh et al., 1997) onboard CLUSTER during a 512 seconds interval just after an inbound shock crossing on February 26 2002 between 22:03 and 22:11 UT (see Figure 11). The Fourier spectrum reveals multiple peaks offering the opportunity to apply the location analysis tool for different frequencies.

During this time the shock regime was quasi-parallel and the spacecraft formation was close to a regular tetrahedron with a minimum spacecraft separation of 87 km and a maximum separation of 135 km. The average plasma flow velocity inferred from the proton bulk velocity measured by the Cluster Ion Spectrometry (CIS) instrument (Rème et al., 1997) was 140 km/s having an orientation of $-45°$ in latitude and $-171°$ in longitude. The average magnetic field was 21 nT, with a direction given by $31°$ latitude and $-89°$ longitude (when not otherwise specified, we use the GSE coordinate system). The maximum variance direction of the magnetic field was closely aligned with the mean magnetic field direction which implies large compressional fluctuations during the selected interval. This justifies the use of the magnetic field magnitude instead

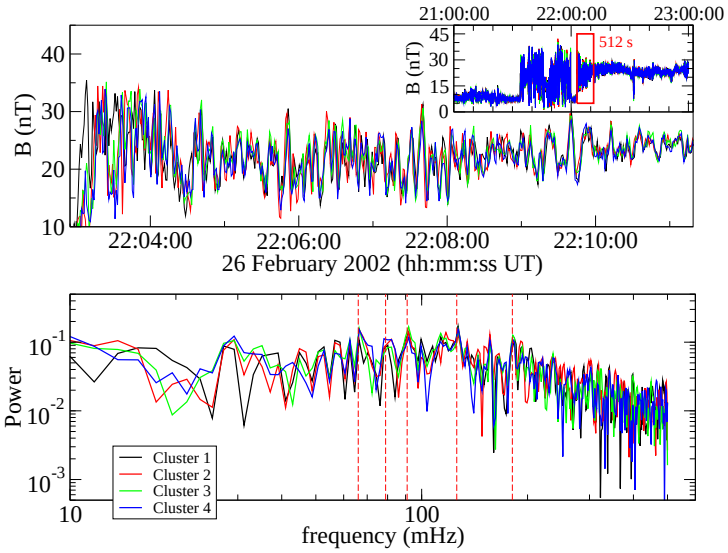

Figure 11: Upper panel: Magnetic field magnitude observed by CLUSTER in the magnetosheath shortly after an inbound shock crossing on 26 February 2002 between 22:03 and 22:11 UT. A two hours overview with the interest interval marked with a red box is shown in the cassette. Lower panel: Frequency power spectrum for the analyzed data interval. The vertical dashed lines indicate the frequencies for which location analysis was performed.

of its components for this case study.

As discussed above, the source locator determines a virtual source defined as the local curvature center of the measured wave fronts. To derive the position of the real source from the position of the virtual one, a wave mode analysis is necessary. This is beyond the purpose of this work. However, despite the fact that it generally has different position in space, the virtual source is an image of the real source and properties like close – remote, static – moving, point source – extended source region are common for the two. Therefore, when we refer to these properties we identify the virtual source with the real source.

The results of location analysis for five different frequencies are listed in Table (6). The array power spectra for $\omega = 181$, 91, and 66 mHz are shown in Figure (12). We have represented the projections of the flow line and of the magnetic field line passing through the identified virtual source position by the dashed, respectively continuous lines in the longitude-latitude plots. The triangles in these plots represent the point of minimum distance between the center of the spacecraft formation and the flow line, respectively the magnetic field line. The squares represent the spacecraft positions. As it can be seen from the k-distance plots, the source is close for the frequency of 66 mHz but is distant – in other words seen as a plane wave by the source locator – for the higher frequencies of 91 mHz and 181 mHz. The grid on which the array power was computed has the same dimensions as for synthetic data, i.e. $30 \times 30 \times 30 \times 30$ for the dimensions distance, latitude, longitude, wave number.

Because of the Doppler effect (equation 25) the measured source frequency

ω (mHz)	distance (km)	$k \times 10^3$ (km^{-1})	longitude (deg)	latitude (deg)	α (deg)
181	> 2000	11.4	-45	10	57
126	> 2000	11.0	-39	4	59
91	> 2000	6.3	-27	7	49
79	759	6.3	-27	-10	65
66	538	5.5	-27	-13	68

Table 6: Results of source location analysis for different frequencies. α is the angle between the line of sight and the plasma flow direction.

is changing as the source moves on its trajectory. If the source comes toward the sensor array, the measured frequency is highest when the source is at the maximum distance and is continuously moving towards lower frequencies as the source is approaching. This means that location analysis performed for different frequencies on the same data interval will reveal different locations of the source corresponding to its motion, allowing us to trace the evolution of the source in time.

In Figure (12) the plot for $\omega = 181$ mHz, the highest frequency in the sequence, shows the power maximum clearly aligned with the magnetic field. The wave source could be a point source moving along the magnetic field but the results from the other frequencies suggest that the measured wave comes rather from a source strongly elongated in the magnetic field direction.

When we move towards lower frequencies, the power maximum changes its shape and aligns itself with the plasma flow direction. At the same time the distance to the virtual source decreases from more than 2000 km to about 500 km. The source seems to move with the plasma flow, approaching the spacecraft formation. This is also consistent with the change in the angle α between the line of sight to the virtual source and the plasma flow direction.

A possible explanation for the change in the alignment of the power maximum is the change in the apparent angular velocity of the source. When the source is far away, its angular velocity is small and it has more time to emit energy from an apparently fixed position. This makes the source to behave more like the static source in Figure (8) and we can resolve its shape. As the source approaches, its angular velocity increases and the source locator will register just the trace of the "brightest" point of the source like in Figure (9).

Quantitatively, the ratio between the angular velocity corresponding to the angles between line of sight and direction of motion α_1 and α_2 is:

$$\frac{v_{\text{ang}}(\alpha_1)}{v_{\text{ang}}(\alpha_2)} = \frac{1 + \tan^2 \alpha_2}{1 + \tan^2 \alpha_1} \tag{36}$$

Applying the above relation we find that the angular velocity corresponding to $\omega = 66$ mHz is more than twice larger than for $\omega = 181$ mHz.

We draw the conclusion that we are tracing one and the same source during its evolution. The measurements are consistent with a source elongated in the magnetic field direction and moving with the plasma flow at close distance to the spacecraft formation.

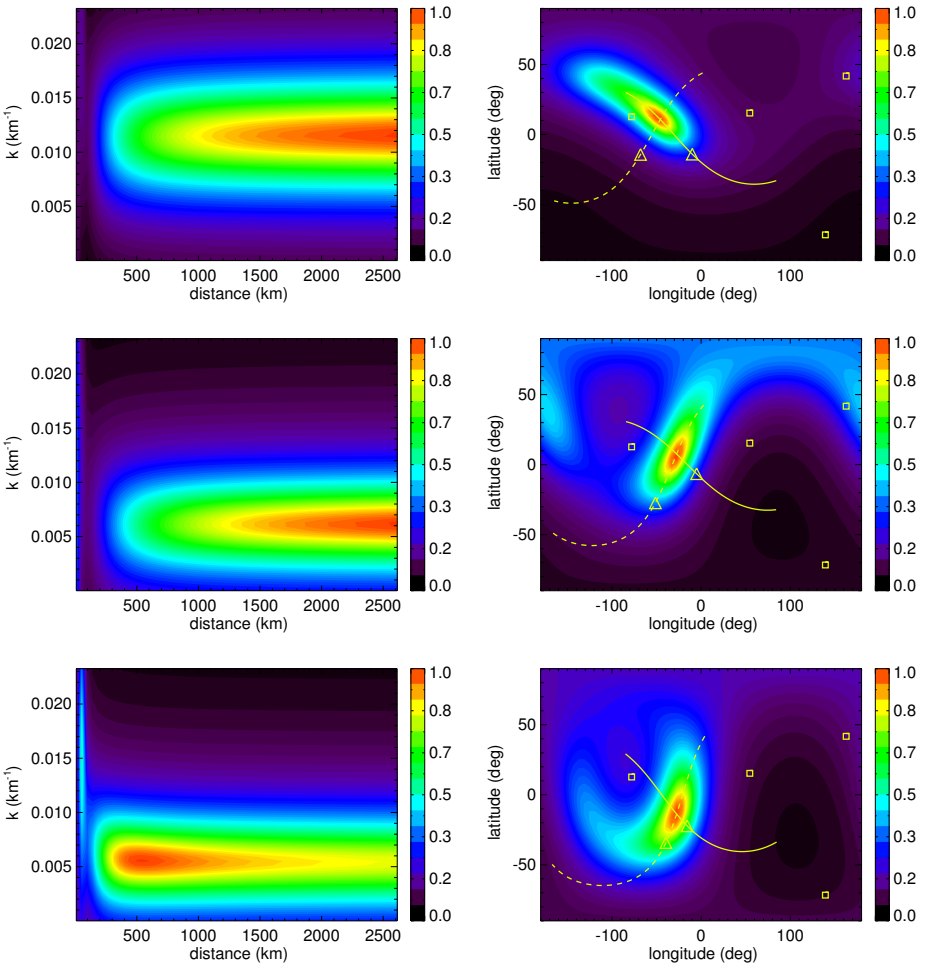

Figure 12: Array power for the magnetic field magnitude measured by CLUSTER. Location analysis is applied to the same 512 seconds data interval for the frequencies (from top to bottom) 181, 91, and 66 mHz. The squares in the longitude-latitude plot represent the spacecraft positions, the continuous lines are the projections of the magnetic field lines passing through the maximum power point. Similarly, the dashed lines represent the plasma flow lines. The triangles on the lines are the points where the distance from the configuration center to the respective line reaches minimum.

5 Conclusions

The source locator is the generalization of the wave telescope technique from the plane waves representation to spherical waves. The new tool decomposes the measured wave field into spherical waves corresponding to virtual sources which would generate the locally detected wave front curvature and the spatial decay of the wave amplitude in an isotropic homogeneous medium. The relation between the virtual source and the real source generating the measured field have to be determined taking into account the wave propagation mode through the medium.

From the shape of the array power maximum and comparing different frequencies the motion of the source can be derived. If the measured waves come from a distributed source region rather than a point source, the source locator can give an indication about its basic geometry.

Using synthetic data we analyzed various cases of source motion relative to the sensor array and/or the plasma background for point and linear sources. We demonstrated that for each of these cases the source locator is able to recover the source position with satisfactory accuracy. While the source locator alone cannot directly differentiate between some situations – as for an example between a linear and a moving point source – comparing the location analysis results for different frequencies or time intervals can help to unambiguously differentiate them.

Using magnetometric CLUSTER data we were able to identify a localized wave source in the day side magnetosheath close to the bowshock. The virtual source region appears to be strongly elongated in the background magnetic field direction and to move with the plasma flow passing close to CLUSTER.

Acknowledgements

The authors would like to thank Kjell Rönnmark and Joachim Vogt for useful discussions at the STIMM workshop in Sinaia. Yasuhito Narita provided a list of bowshock crossings from which we selected the event presented here. We like to thank the two reviewers for very interesting discussions. This work was financially supported by the German Bundesministerium für Wirtschaft und Technologie and the Deutsches Zentrum für Luft und Raumfahrt under contract 50OC0103.

References

Balikhin, M. A., Pokhotelov, O. A., Walker, S. N., and Andre, M. (2003). Identification of low frequency waves in the vicinity of the terrestrial bow shock. *Planetary and Space Science*, 51:693–702.

Balogh, A., Dunlop, M. W., Cowley, S. W. H., Southwood, D. J., Thomlinson, J. G., Glassmeier, K. H., Musmann, G., Luhr, H., Buchert, S., Acuna, M. H., Fairfield, D. H., Slavin, J. A., Riedler, W., Schwingenschuh, K., and Kivelson, M. G. (1997). The Cluster Magnetic Field Investigation. *Space Science Reviews*, 79:65–91.

Capon, J., Greenfield, R. J., and Kloker, R. J. (1967). Multidimensional maximum-likehood processing of a large aperture seismic array. In *Proc. IEEE, Volume 55*, pages 192–213.

Escoubet, C. P., Schmidt, R., and Goldstein, M. L. (1997). Cluster: Science and Mission Overview. *Space Sci. Rev.*, 79:11–32.

Glangeaud, F. and Latombe, C. (1983). Identification of electromagnetic sources. *Annales Geophysicae*, 1:245–251.

Glassmeier, K.-H. (1980). Magnetometer array observations of a giant pulsation event. *Journal of Geophysics*, 48:127–138.

Glassmeier, K.-H., Motschmann, U., Dunlop, M., Balogh, A., Acuña, M. H., Carr, C., Musmann, G., Fornaçon, K.-H., Schweda, K., Vogt, J., Georgescu, E., and Buchert, S. (2001). Cluster as a wave telescope - first results from the fluxgate magnetometer. *Annales Geophysicae*, 19:1439–1447. Correction, Annales Geophysicae, 21, 1071, 2003.

Küppers, F., Untiedt, J., Baumjohann, W., Lange, K., and Jones, A. G. (1979). A two-dimensional magnetometer array for ground-based observations of auroral zone electric currents during the international magnetospheric study. *Journal of Geophysics*, 46:429–450.

Lefeuvre, F. and Pinçon, J. L. (1992). Determination of the wave-vector spectrum for plasma waves and turbulence observed in space plasmas. *Journal of Atmospheric and Terrestrial Physics*, 54:1227–1235.

Motschmann, U., Woodward, T. I., Glassmeier, K.-H., and Dunlop, M. W. (1995). Array Signal Processing Techniques. In Glassmeier, K.-H., Motschmann, U., and Schmidt, R., editors, *Proc. CLUSTER Workshop on Data Analysis Tools*, pages 79–86. ESA.

Narita, Y., Glassmeier, K.-H., Schäfer, S., Motschmann, U., Sauer, K., Dandouras, I., Fornaçon, K.-H., Georgescu, E., and Rème, H. (2003). Dispersion analysis of ULF waves in the foreshock using cluster data and the wave telescope technique. *Geophys. Res. Lett.*, 30:43–1.

Neubauer, F. M. and Glassmeier, K. H. (1990). Use of an array of satellite as a wave telescope. *J. Geophys. Res.*, 95:19115–19122.

Pillai, S. U. (1989). *Array signal processing*. Springer.

Pinçon, J. L. and Lefeuvre, F. (1991). Local characterization of homogeneous turbulence in a space plasma from simultaneous measurements of field components at several points in space. *J. Geophys. Res.*, 96:1789–1802.

Pinçon, J. L. and Lefeuvre, F. (1992). The application of the generalized Capon method to the analysis of a turbulent field in space plasma - Experimental constraints. *Journal of Atmospheric and Terrestrial Physics*, 54:1237–1247.

Pinçon, J. and Motschmann, U. (1998). Multi-Spacecraft Filtering: General Framework. In Paschmann, G. and Daly, P., editors, *Analysis methods for multi-spacecraft data*, ISSI Sci. Rep. SR-001, pages 65–78. ISSI, Bern.

Rème, H., Bosqued, J. M., Sauvaud, J. A., Cros, A., Dandouras, J., Aoustin, C., Bouyssou, J., Camus, T., Cuvilo, J., Martz, C., Medale, J. L., Perrier, H., Romefort, D., Rouzaud, J., d'Uston, C., Mobius, E., Crocker, K., Granoff, M., Kistler, L. M., Popecki, M., Hovestadt, D., Klecker, B., Paschmann, G., Scholer, M., Carlson, C. W., Curtis, D. W., Lin, R. P., McFadden, J. P., Formisano, V., Amata, E., Bavassano-Cattaneo, M. B., Baldetti, P., Belluci, G., Bruno, R., Chionchio, G., di Lellis, A., Shelley, E. G., Ghielmetti, A. G., Lennartsson, W., Korth, A., Rosenbauer, H., Lundin, R., Olsen, S., Parks, G. K., McCarthy, M., and Balsiger, H. (1997). The Cluster Ion Spectrometry (CIS) Experiment. *Space Science Reviews*, 79:303–350.

Robert, P., Roux, A., Harvey, C. C., Dunlop, M. W., Daly, P. W., and Glassmeier, K.-H. (1998). Tetrahedron geometric factors. In *Analysis methods for multi-spacecraft data*, pages 323–348. Int. Space Sci. Inst., Bern, Switzerland.

Sahraoui, F., Pinçon, J. L., Belmont, G., Rezeau, L., Cornilleau-Wehrlin, N., Robert, P., Mellul, L., Bosqued, J. M., Balogh, A., Canu, P., and Chanteur, G. (2003). ULF wave identification in the magnetosheath: The k-filtering technique applied to Cluster II data. *J. Geophys. Res.*, 108(A9):1335.

Samson, J. C. (1983). The spectral matrix, eigenvalues, and principal components in the analysis of multichanel geophysical data. *Annales Geophysicae*, 1:115–119.

Santolík, O. and Gurnett, D. A. (2002). Propagation of auroral hiss at high altitudes. *Geophys. Res. Lett.*, 29:119–1.

Schäfer, S., Glassmeier, K.-H., Narita, Y., Fornaçon, K.-H., Dandouras, I., and Fränz, M. (2005). Statistical Phase Propagation and Dispersion Analysis of low Frequency Waves in the Magnetosheath. *Annales Geophysicae*, 23:3338–3349.

Storey, L. R. O. and Lefeuvre, F. (1979). The analysis of 6-component measurements of a random electromagnetic wave field in a magnetoplasma, i, the direct problem. *Geophys. J. R. Astron. Soc.*, 56:255–270.

Storey, L. R. O. and Lefeuvre, F. (1980). The analysis of 6-component measurements of a random electromagnetic wave field in a magnetoplasma, ii, the integration kernels. *Geophys. J. R. Astron. Soc.*, 62:173–194.

Tjulin, A., Pinçon, J.-L., Sahraoui, F., André, M., and Cornilleau-Wehrlin, N. (2005). The k-filtering technique applied to wave electric and magnetic field measurements from the Cluster satellites. *Journal of Geophysical Research (Space Physics)*, 110(A9):11224–+.